Photochemical & Photobiological Sciences

RSC Publishing

PAPER

View Article Online
View Journal | View Issue

Cite this: *Photochem. Photobiol. Sci.*, 2013, **12**, 1375

A joint experimental/theoretical study of the ultrafast excited state deactivation of deoxyadenosine and 9-methyladenine in water and acetonitrile†‡

Thomas Gustavsson,*[a] Nilmoni Sarkar,[b] Ignacio Vayá,[c] M. Consuelo Jiménez,[c] Dimitra Markovitsi[a] and Roberto Improta*[d]

Received 20th February 2013,
Accepted 27th March 2013

DOI: 10.1039/c3pp50060h

www.rsc.org/pps

The excited states of deoxyadenosine (dA) and 9-methyladenine (9Me-Ade) were studied in water and acetonitrile by a combination of steady-state and time-resolved spectroscopy and quantum chemical calculations. Femtosecond fluorescence upconversion experiments show that the decays of dA and 9Me-Ade after excitation at 267 nm are very similar, confirming that 9Me-Ade is a valid model for the calculations. The fluorescence decays can be described by an ultrafast component (<100 fs) and a slower one (≈ 300–500 fs); they are slightly slower in acetonitrile than in water. Time-dependent DFT calculations on 9Me-Ade, using PBE0 and M052X functionals and including both bulk and specific solvent effects, provide absorption and emission spectra in good agreement with experiments, giving a comprehensive description of the decay mechanism. It is shown that, in the Franck–Condon region, the lowest in energy state is the optically bright L_a state, with the L_b state situated about 2000 cm^{-1} higher. Both states are populated when excited at 267 nm, but the L_b state undergoes an ultrafast $L_b \rightarrow L_a$ decay, too fast for our time-resolution (≈ 80 fs). This is confirmed by the experimentally observed fluorescence anisotropies, attaining values lower than 0.4 already at time zero. Consequently, the ensuing excited state relaxation mechanism can be described as the evolution along an almost barrierless path from the Franck–Condon region of the L_a potential energy surface towards a conical intersection with the ground state. This internal conversion mechanism proceeds without any significant involvement of any near-lying nπ* state.

1. Introduction

Nucleic acids strongly absorb UV light and this process is potentially dangerous since it can trigger a cascade of photochemical events leading to the damage of the genetic code, giving rise to carcinogenesis and apoptosis. As a consequence, a large number of experimental and computational studies (too many to be exhaustively reviewed in this paper) have been devoted to the study of the excited state dynamics of DNA, model oligonucleotides and the monomeric nucleobases.[1–8]

One of the major outcomes of these studies is that the excited state deactivation of the monomers is extremely efficient, proceeding on a sub-picosecond time-scale, while for the helices it is much more complex, ranging from the femtosecond to the nanosecond timescale, depending on the system.[9,10] For the monomers, detailed theoretical studies have shown that the ultrafast internal conversion proceeds through Conical Intersections (CIs).[4] For the helices, part of the explanation can be found in the population of excitonic states[11–13] and/or charge transfer states.[14–16] However, the presence of 'monomer-like' deactivation channels within single and double strands is still a subject of much discussion. For example, the excited state decay mechanism in the adenine monomer has been proposed to be operative also within single and double adenine strands.[17] Beyond their inherent interest, nucleobases also serve as an important source of information on the subtle interplay of various effects (molecular structure, solvent, substituents, excitation wavelength, pH) that govern the excited state dynamics of organic molecules in general.

[a]*CNRS, IRAMIS, SPAM, Francis Perrin Laboratory, URA 2453, 91191 Gif-sur-Yvette, France. E-mail: thomas.gustavsson@cea.fr*
[b]*Department of Chemistry, Indian Institute of Technology, Kharagpur 721302, WB, India*
[c]*Department of Chemistry, Universitat Politècnica de València, 46022 Valencia, Spain*
[d]*Instituto Biostrutture e Biommagini-CNR Via Mezzocannone 16, I-80134 Napoli, Italy. E-mail: robimp@unina.it*
†This article dedicated to Prof. Miguel A. Miranda on the occasion of his 60th birthday.
‡Electronic supplementary information (ESI) available. See DOI: 10.1039/c3pp50060h

In this respect, the adenine (Ade) chromophore displays a complicated behaviour, typical of the DNA bases, characterized by an ultrafast excited state decay both in gas phase and solution, rendering their interpretation very difficult. The reason for this is, as outlined below, the competition between different highly efficient non-radiative processes. A first point to consider is already the complexity of the lowest energy absorption band of Ade. While vapour absorption spectra only show one absorption band with a maximum at 252 nm (4.92 eV),[18] subsequent molecular beam experiments have revealed that there are several close-lying excited states (five resolved vibronic bands in the range of 4.40–4.55 eV).[19–25]

Quantum mechanical (QM) computations in the gas phase indeed show that three different singlet excited states lie close in energy in the Franck–Condon (FC) region, one dark with nπ* character (HOMO − 1 → LUMO, hereafter labelled as $S_{n\pi^*}$) and two bright ππ* excited states (L_a and L_b). The L_a excited state corresponds mainly to a HOMO → LUMO excitation and carries most of the oscillator strength. The L_b excited state results from the combination of HOMO − 2 → LUMO and HOMO → LUMO + 1 excitations and is consequently characterized by a much smaller oscillator strength. In the gas phase $S_{n\pi^*}$ should be the lowest energy excited states, whereas the energy ordering between L_a and L_b (which are within 0.2 eV) depends on the adopted computational method.[26–29] Different possible decay pathways have been identified for these excited states and multiple crossings characterized. In particular, two critical CIs have been located between the lowest energy adiabatic states and S_0, involving the out-of-plane motion of the C2-H group (see Fig. 1 for atom labelling), usually labelled ^{2}E, and the out-of-plane motion of the C6-NH_2 group, labelled $^6S_1$.[27–29] The ^{2}E CI has been associated with the L_a state, while the $^6S_1$ CI concerns the $S_{n\pi^*}$ state. However, for a non-planar geometry the nπ* and ππ* states are strongly mixed and it is therefore not easy to assign a well-defined diabatic state to the different adiabatic states. In this scenario, it is not surprising that the excited state decay is multi-exponential and strongly dependent on the excitation wavelength.[30–35] The experimentally determined lifetimes vary from case to case, but, basically, there is an ultrafast component ($\tau_1 \sim 0.1$ ps) and a slower one ($\tau_2 \sim 0.75$–1 ps). The assignment of these decay constants has been strongly debated.[26–29,36–42] The fast component (τ_1) is ascribed to direct $L_a \rightarrow S_0$ decay[27] or to an underlying state ($L_a \rightarrow S_{n\pi^*}$ or $L_a \rightarrow L_b$),[42] while the slower one (τ_2) is assigned to S_0 recovery from the latter states (with special emphasis on the $S_{n\pi^*} \rightarrow S_0$ decay).[36,37,42] It has also been proposed that both τ_1 and τ_2 are associated with the $L_a \rightarrow S_0$ decay.[29] Finally, for higher excitation energies a deactivation channel involving the breaking of the N9–H bond should be active, accessed through a Rydberg πσ* state ($L_a \rightarrow \pi\sigma^* \rightarrow S_0$).[26]

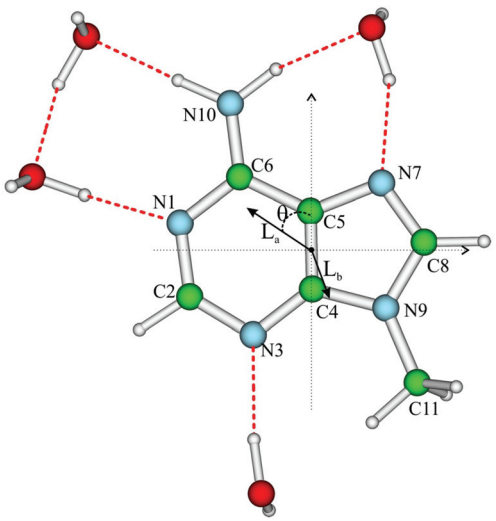

Fig. 1 Schematic drawing and atom labelling of the 9Me-Ade $4H_2O$ model used to study the excited state decay in water. Also shown are the transition dipole moment orientations of the two bright ππ* states L_a and L_b. These are defined relative to the short molecular axis.

A number of steady-state spectroscopic studies have been dedicated to the spectroscopy of Ade in water as well as other environments and it is not our intention to present an exhaustive review here. It should be remarked, however, that much confusion has been caused by the fact that two adenine tautomers, the major 9(H)- and the minor 7(H)-tautomers, are present in solution. We will in the following only focus on the canonical 9(H)-adenine tautomer, denoted "adenine" if not otherwise stated. Experimentally, this limits the scope to 9-substituted adenines such as adenosine (Ado), deoxyadenosine (dA) or 9-methyladenine (9Me-Ade). The first absorption band of Ado in room-temperature water has its maximum at 260 nm (4.77 eV), implying that it is red-shifted by 0.15 eV with respect to the gas phase.[18,43] This band has no apparent sub-structure[18,43,44] but is known to be composed of two ππ* electronic transitions.[45] These two transitions have notably been resolved by magnetic circular dichroism in aqueous solution, giving the values of 272 nm (4.56 eV) and 253 nm (4.90 eV).[46] The existence of two ππ* electronic transitions was independently shown in linear dichroism measurements of 9-methyladenine in stretched polymer films.[47]

The presence of possible low-lying nπ* states has been widely discussed in the past, but no unambiguous observation has been reported and the location of nπ* states in room-temperature solutions still remains unclear. It is worthwhile to remark that, in their transient absorption experiments on various nucleotides in aqueous solution, Kohler and coworkers observed long-lived decay components for the pyrimidines, assigned to nπ* states, but not for the purines, and in particular not for adenosine monophosphate (AMP).[48]

In this respect, quantum chemistry calculations predict that $S_{n\pi^*}$ is destabilized with respect to L_a and L_b in water. More precisely, the energy ordering predicted at the CASSCF level for adenine in water, including the solvent effect by means of a Linear Response Free Energy Procedure, strongly depends on the geometry chosen for the S_0 minimum.[49] For a C_s planar minimum it is $L_a < L_b < S_{n\pi^*}$ while for a C_1 minimum it $L_b < S_{n\pi^*} < L_a$. A Monte Carlo MM/CASPT2 study[50] indicates that in water solution the $S_{n\pi^*}$ is blue-shifted by 0.58 eV with respect to the gas phase, while L_b and L_a are

red-shifted by 0.17 and 0.34 eV, respectively, resulting in an energy ordering $L_b \sim L_a < S_{n\pi^*}$. Based on a multireference perturbed CI approach coupled with PCM, it was predicted that for 9(H)-adenine in water, $L_b < L_a < S_{n\pi^*}$, with L_a and L_b experiencing a substantial red-shift with respect to the gas phase results and $S_{n\pi^*}$ a weak blue-shift.[51] TD-DFT/PCM calculations on different Ade derivatives (9-methyladenine, 9Me-Ade, dA, dAMP) show that $S_{n\pi^*}$ is significantly destabilized with respect to the gas phase, while L_a and L_b exhibit weak red-shifts.[52] MM/QM calculations by Thiel and co-workers,[53] including water molecules at the MM level while treating Ade by the OM2/MRCI semiempirical method and taking into account the thermal motion of the system, provide similar indications, with $S_{n\pi^*}$ blue-shifted by 0.1/0.3 eV with respect to the gas phase and L_a red-shifted by 0.1 eV. In the latter study, however, significant mixing of the different diabatic states in the FC region is found. Finally, by means of CASPT2/MM calculations, Garavelli and co-workers found that for one adenine molecule (treated at CASPT2//CASSCF(12,10)/ANO-l level) embedded in a $(dA)_{10}$ single strand in water (treated at the MM level) L_a is the lowest energy excited state, while $S_{n\pi^*}$ is 0.5/0.7 eV less stable.[54] On the basis of this short review, it is clear that, despite the quantitative differences between the methods, the solvent significantly affects the relative stability of the lowest energy excited state of Ade and that explicit inclusion of solute–solvent interactions is particularly important, especially for determining the relative stability of $S_{n\pi^*}$ in water.

About a decade ago, the ultrafast decay of the adenosine S_1 state in water was determined independently by femtosecond transient absorption[55] and fluorescence upconversion[56] experiments. Subsequent time-resolved fluorescence measurements with improved time-resolution showed that the excited state decay is not mono-exponential but contains an ultrafast component (<0.1 ps) and a slower one (~0.5 ps).[57–59] Based on the previous interpretation of linear dichroism data,[47] Kwok *et al.* assigned the two times to the L_a and L_b states with the fast component reflecting the $L_a \rightarrow L_b$ relaxation.[59] The time-zero fluorescence anisotropy, which is a very sensitive measure of changes in the electronic structure of the emitting state, was found to be about 0.24.[58] This is much lower than the theoretical limit of 0.4 for parallel absorption and emission transition dipoles, confirming the presence of an electronic relaxation preceding the emission.

In parallel, time-resolved experiments on natural adenine (containing both 9(H)- and 7(H)-adenine) in water showed that the excited state decay is clearly bi-exponential, with a long component of about 8 ps and a faster one of a few hundreds femtoseconds.[57,60] The long component was assigned to the 7(H) tautomer while the fast one was assigned to the canonical 9(H) tautomer. This assignment was corroborated by the comparison between the excited state lifetimes of 9Me-Ade and 7-methyladenine (7Me-Ade): the former is 0.22 ± 0.02 ps, and the latter is 4.23 ± 0.13 ps.[61] Solvent effects were also studied; in acetonitrile, the lifetimes of 7Me-Ade and 9Me-Ade were found to be (3.3 ± 0.3 ps) and (0.35 ± 0.02 ps), respectively. Interestingly, the lifetimes in acetonitrile seem to be longer than those observed in water. This is contrary to what was observed for uracil and thymine in water and acetonitrile solutions.[62–64]

These results have been interpreted in different ways. Indeed the above mentioned QM/MM surface hopping simulations have predicted that ground state recovery occurs with a time constant of 410 fs, mainly through the $S_{n\pi^*}/S_0$ CI ($^6S_1$), following the same $L_a \rightarrow S_{n\pi^*} \rightarrow S_0$ mechanism predicted by the same method in the gas phase.[53] Alternatively, it has been proposed that in aqueous solution the most important non-radiative deactivation path involves a direct $L_a \rightarrow S_0$ decay, *via* the ^{2}E CI.[49,54]

It is clear that several key issues concerning the excited state dynamics of adenine derivatives in solution are still open, from the excited state ordering in the FC region to the deactivation mechanism. We have therefore decided to revisit the excited state decay of adenine derivatives, combining femtosecond fluorescence upconversion experiments with an improved time-resolution (350 fs full width at half maximum (fwhm) instead of 450 fs) on dA and 9Me-Ade and quantum mechanical TD-DFT calculations on 9Me-Ade. According to our previous studies, solvent effects can provide very useful information on the excited state decay mechanism of nucleobases.[63–67] We have therefore characterized the excited state dynamics of dA and 9Me-Ade in two different solvents, water and acetonitrile, the former protic and the latter aprotic. This is very important since solute–solvent hydrogen bonding has been shown to play a crucial role in the energetic ordering of different electronic states, particularly $n\pi^*$ states, of the nucleobases.[4] We also pay particular attention to the fluorescence anisotropy and its wavelength dependence, since this is a sensitive probe of the electronic nature of the emitting state.

2. Material and methods

2.1. Experimental details

Deoxyadenosine (dA) was purchased from Sigma and 9-methyladenine (9Me-Ade) from Aldrich. Acetonitrile was purchased from Sigma-Aldrich and ultrapure water was obtained from a Millipore Milli-Q apparatus. All products were used without further purification.

Absorption spectra were recorded with a Perkin-Elmer Lambda 900 spectrophotometer using 1 mm quartz cells (QZS). Fluorescence spectra (5 nm bandpass) were recorded with a SPEX Fluorolog-3 spectrofluorometer using a 1 cm × 1 cm quartz cell. The light source was a 450 Watt arc Xenon lamp.

The femtosecond fluorescence upconversion setup has been described earlier.[68] Briefly, the excitation source is the third harmonic at 267 nm of a mode-locked Ti-sapphire laser (120 fs, 800 nm, 76 MHz). Typically, the average excitation power used was about 40 mW. Fluorescence decays were recorded at various wavelengths between 310 and 550 nm with a sufficiently small time-step to determine the apparatus

function. Parallel ($I_{par}(t)$) and perpendicular ($I_{perp}(t)$) excitation/detection configurations were realized by controlling the polarization of the exciting beam with a zero-order half-wave plate. All measurements were performed at room temperature (20 ± 1 °C) under aerated conditions. Solutions (≈ 2.5 × 10^{-3} mol dm^{-3}) were kept flowing through a 1.0 mm quartz cell, which itself was kept in continuous motion perpendicular to the excitation beam. The power density cannot be measured precisely within the excitation volume but we estimate it to be 0.2 ± 0.1 GW cm^{-2} for a 40 mW output from the tripler unit (assuming a 40 micron diameter of the focused beam).

Total fluorescence kinetics $F(t)$ shown below were constructed from the parallel and perpendicular signals ($I_{par}(t)$ and $I_{perp}(t)$) according to the equation:

$$F(t) = I_{par}(t) + 2I_{perp}(t) \quad (1)$$

Likewise, the fluorescence anisotropy $r(t)$ is given by the expression

$$r(t) = (I_{par}(t) - I_{perp}(t))/F(t) \quad (2)$$

In order to evaluate the characteristic times involved, instead of treating $F(t)$ and $r(t)$ separately we performed a merged nonlinear fitting/deconvolution process using the impulse response model functions

$$i_{par}(t) = (1 + 2r(t))f(t) \quad (3)$$

$$i_{perp}(t) = (1 - r(t))f(t) \quad (4)$$

convoluted by the Gaussian instrument response function, $I(t) \propto i(t) \otimes G(t)$. The model functions thus obtained were fitted to the experimentally measured (I_{par}) and (I_{perp}) signals. The fwhm value of a Gaussian apparatus function was found to be about 350 fs fwhm at 330 nm which is better than in our previous studies (450 fs fwhm).[57,58] A figure showing the improved performances of the setup is shown in the ESI (Fig. S1‡). We judged that the time resolution of our setup is ≈80 fs after deconvolution, but the actual value depends on the wavelength, the relative amplitude and the signal-to-noise ratio.

2.2. Computational details

Geometry optimizations have been performed in aqueous solution at the PCM/DFT/6-31G(d) level for the ground and at PCM/TD-DFT/6-31G(d) level for the excited state, exploiting PBE0,[69] M052X,[70] and CAM-B3LYP[71] functionals. The PBE0 hybrid functional,[69] despite the absence of adjustable parameters, has shown remarkable accuracy in the treatment of excited states.[72,73] Concerning the photophysics of nucleobases, PCM/PBE0 calculations provide Vertical Excitation and Emission Energies very close to the experimental band maxima (within 0.15 eV) both for pyrimidine[62,65,74] and for purine.[52,75,76] Our computational results in the gas phase are also in good agreement with those obtained by using sophisticated post-HF methods. M052X provides a similar description of the lowest energy excited states of nucleobases, and it is not plagued by the deficiencies of the standard density functional in the treatment of CT transitions, as shown by our studies on oligoadenine stacked oligomers.[16,77–82]

The effect of basis set extension on the absorption and emission energies has been estimated by test computations with more extended 6-31+G(d,p) and 6-311+G(2d,2p) basis sets.

Bulk solvent effects have been included by the polarizable continuum model (PCM),[83] resorting both to the 'standard' LR (linear-response) implementation of PCM/TD-DFT, for which analytical gradients are available,[84] and to the State-Specific (SS) implementation of PCM/TD-DFT, allowing for a more accurate determination of the relative energy of different excited states.[85,86] The effect of explicit solute–solvent interaction in a hydrogen bonding solvent such as water has been studied by including four water molecules of the first solvation shell. We have checked that our results are not qualitatively affected by changes in the number and in the coordination geometry of the water molecules. All the calculations have been performed by using the Gaussian09 package.[87]

3. Results

3.1. Experimental results

Normalized steady-state absorption and corrected fluorescence spectra (λ_{exc} = 255 nm) of dA and 9Me-Ade in water and acetonitrile are shown in Fig. 2. In order to facilitate comparisons with the results of calculations they are here shown on a wavenumber scale (the fluorescence spectra being scaled by a factor λ^2). The fluorescence spectra were smoothed over a few data points. The corresponding spectra on a wavelength scale are given in the ESI (Fig. S2‡).

In order to obtain a more quantitative description of the spectral characteristics, spectra (for absorption, the first absorption band around 260 nm) were fitted by single lognormal functions. The fitted absorption spectra together with deviations are given in the ESI (Fig. S3‡). The absorption maximum for dA in water is 38.5 × 10^3 cm^{-1} (260 nm) while that of 9Me-Ade is slightly red-shifted to 38.3 × 10^3 cm^{-1} (261 nm). For both molecules the absorption maximum in

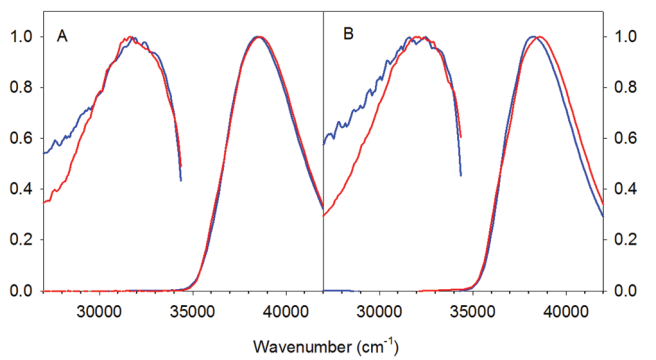

Fig. 2 Normalized steady-state absorption and fluorescence spectra of (A) dA in water (blue) and acetonitrile (red), (B) 9Me-Ade in water (blue) and acetonitrile (red).

CH_3CN is 38.6×10^3 cm^{-1} (259 nm). The widths of the absorption spectra are all around 4.6×10^3 cm^{-1} (fwhm) except that of 9Me-Ade in CH_3CN which is slightly narrower ($\sim 4.3 \times 10^3$ cm^{-1} fwhm). The lognormal fits are fully adequate, showing no sign of more than one transition, in line with previous reports.[18,43,44] Even though a decomposition into two separate bands (corresponding to L_a and L_b) is technically possible,[11,47,59] there is no direct experimental support for this.

The fluorescence maxima of the four studied systems are all very close, peaking at $\sim(32.0 \pm 0.3) \times 10^3$ cm^{-1} ($\sim 308 \pm 3$ nm). All fluorescence spectra extend far beyond 400 nm but the shapes differ radically between water and CH_3CN solutions. The fluorescence spectra are significantly broader in water ($\sim 8.0 \times 10^3$ cm^{-1} fwhm) than in CH_3CN ($\sim 5.8 \times 10^3$ cm^{-1} fwhm). The Stokes shifts are large, ranging from $\sim 5.8 \times 10^3$ cm^{-1} for 9Me-Ade in H_2O to $\sim 6.5 \times 10^3$ cm^{-1} for dA in CH_3CN. However, these small variations are within the experimental error bars. The use of a lognormal function to describe the fluorescence spectra is adequate and the red wing is poorly accounted for. A decomposition of the fluorescence spectra into two separate bands (corresponding to L_a and L_b) has been proposed in the literature.[59] We have also tried such an approach in the present case, but without success. The fitted fluorescence spectra together with deviations are given in the ESI (Fig. S4‡).

Total fluorescence decays of 9Me-Ade in water and of dA in acetonitrile measured at various wavelengths after excitation at 267 nm are shown in Fig. 3. Corresponding traces of 9Me-Ade in acetonitrile and of dA in water are given in the ESI (Fig. S5‡). As can be seen in Fig. 3, the decays become slightly longer with increasing wavelength. This is indeed the case for all the four solute–solvent systems studied.

Interestingly, the fluorescence decays of 9Me-Ade and dA in water measured in the visible spectral region (450–550 nm) are still sub-picosecond (Fig. S6‡), only slightly longer than in the UV. This is contrary to what was observed for dGMP for which the fluorescence decays in the visible were much longer, characterized by a 2 ps time constant.[88] For comparison, at 500 nm and 1 ps, the fluorescence trace of dA/H_2O has lost 83% of its initial intensity while that of dGMP/H_2O has only lost about 40%.

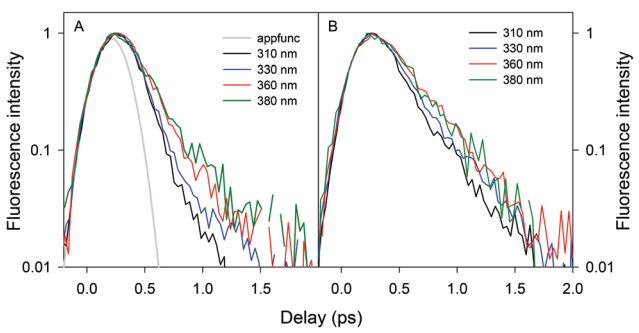

Fig. 3 Total fluorescence decays at various wavelengths of (A) 9Me-Ade in water and (B) dA in acetonitrile. The apparatus-function is shown in grey.

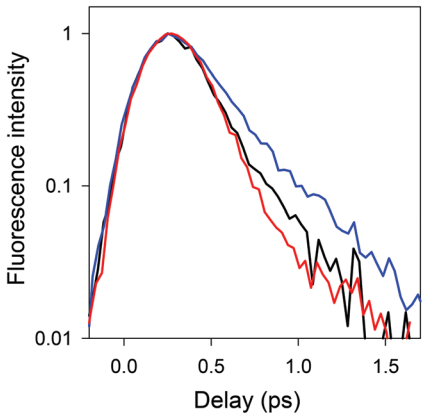

Fig. 4 Total fluorescence decays at 330 nm of 9Me-Ade in water (red), dA in water (black) and dA in CH_3CN (blue).

Table 1 Average fluorescence decay times (in ps) of the fluorescence decays of dA and 9Me-Ade in H_2O and CH_3CN after excitation at 267 nm. See text for details

	dA		9Me-Ade	
	H_2O	CH_3CN	H_2O	CH_3CN
310 nm	0.11 ± 0.02	0.18 ± 0.02	0.10 ± 0.02	0.12 ± 0.02
330 nm	0.12 ± 0.03	0.24 ± 0.03	0.13 ± 0.01	0.15 ± 0.03
360 nm	0.20 ± 0.03	0.31 ± 0.09	0.15 ± 0.02	0.21 ± 0.04
380 nm	0.27 ± 0.01	0.33 ± 0.01	0.24 ± 0.01	0.30 ± 0.01

For both 9Me-Ade and dA, the fluorescence decay at a given wavelength is slightly longer in CH_3CN than in water. This is illustrated in Fig. 4, where the fluorescence decays at 330 nm of 9Me-Ade and dA in water as well as dA in acetonitrile are compared. Similar results were obtained at the other wavelengths.

In order to quantify the time-resolved signals, experimental data were treated in a nonlinear fitting/deconvolution process as described by eqn (3) and (4) above. Free-floating bi-exponential functions $(\alpha \exp(-t/\tau_1) + (1 - \alpha)\exp(-t/\tau_2))$ were used for the total intensity decay $f(t)$ while the anisotropy was described by a free-floating constant r_0. The fluorescence decays are dominated by an ultrafast component, ~100 fs, and a slower one, ranging from about 300 to 500 fs depending on the wavelength. Due to the high correlation between the parameters, it is more instructive to use the average decay time, $\langle\tau\rangle$, defined as $\alpha\tau_1 + (1 - \alpha)\tau_2$, reported in Table 1. Resulting characteristic decay times from the bi-exponential fits are given in Table S1 (ESI‡). Fitted decay times of the fluorescence decays at 450 nm for 9Me-Ade and dA in water are also given in Table S1.‡

Comparing the various average lifetimes confirms the observations made above; that is, the fluorescence decay at a given wavelength is slightly longer in CH_3CN than in water. The largest difference is observed for dA at 330 nm, where the average decay in water is ~120 fs while it is ~240 fs in acetonitrile. The same trends can be observed at 310 and 360 nm.

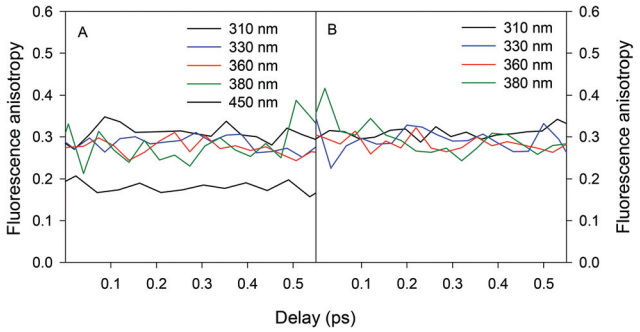

Fig. 5 Fluorescence anisotropy decays of (A) 9Me-Ade in water and (B) dA in acetonitrile.

At 380 nm a mono-exponential model function suffices to describe the experimental curves.

The fluorescence anisotropy, determined from the same data used for Fig. 3, that is, 9Me-Ade in water and dA in acetonitrile at various wavelengths, is shown in Fig. 5. The curves are truncated at 0.55 ps, beyond which the signal-to-noise ratio becomes increasingly poorer. Similar results were also obtained for dA in water and 9Me-Ade in acetonitrile (not shown).

As can be seen, the anisotropies below 380 nm are constant within the studied time-window and wavelength-independent within the uncertainty limits. An average value of $r = 0.29 \pm 0.03$ can be deduced. This is significantly less than the theoretical limit of 0.4 for parallel absorption and emission transition dipoles. We would like to remark that, owing to the improved experimental setup, these values are slightly higher than the value of 0.24 reported earlier.[58] Fluorescence anisotropies in the visible are substantially lower. An example is given in Fig. 5, where the signal of 9Me-Ade in water at 450 nm, having an average value of 0.18 ± 0.02, is shown.

A population transfer between L_b and L_a will result in decay of the fluorescence anisotropy, since the emission dipoles of the L_a and L_b states are nearly perpendicular. Interestingly, we do not observe any rapid component in the fluorescence anisotropy decays; they start out from about 0.3 already at time zero. This can be taken as a sign that the interconversion between L_b and L_a is much faster than our time-resolution (<80 fs), implying that L_b does not contribute to the observed fluorescence.

The results of the steady-state and time-resolved experiments described above show that the properties of dA and 9Me-Ade are very similar, suggesting that 9Me-Ade can be used with confidence in the modeling to interpret the photophysics of the adenine chromophore.

3.2. Computational results

Absorption spectra and the Franck–Condon region. Confirming a previous analysis, according to PCM/PBE0 calculations the lowest energy excited state in aqueous solution is L_a, with L_b being 2000 cm^{-1} and $S_{n\pi^*}$ 4000–5000 cm^{-1} (depending on the basis set) less stable than L_a. As reported in Table 2 and shown in Fig. 1, L_a is mainly polarized along the long molecular axis, L_b along the short one and $S_{n\pi^*}$ perpendicularly to the molecular plane. The computed E_V of the brightest L_a transition at the PBE0/6-31G(d) level is 41 100 cm^{-1} ($\lambda_A \sim 240$ nm), *i.e. ca.* 2800 cm^{-1} blue-shifted with respect to the experimental absorption maximum. A significant part of this discrepancy is recovered by increasing the basis set, which is only ~1200 cm^{-1} at the 6-311+G(2d,2p) level. In any case, vibrational effects should be considered to predict the optical line-shape and, consequently, the absorption maximum[89] (not to mention the contribution of L_b to the absorption spectrum).

Table 2 Main features of the lowest energy excited states of 9Me-Ade in water solution, according to LR-PCM/PBE0 calculations on the 9Me-Ade·4H_2O model. PCM/PBE0/6-31G(d) geometry optimizations. Excitation energy (E_V) in cm^{-1}. Dipole moment (μ) in Debye

	6-31G(d)	6-31G(d) SS[a]	6-31+G(d,p)	6-311+G(2d,2p)
L_a				
E_V (osc.str)	41 100(0.25)	41 600(0.17)	40 200(0.30)	39 700(0.30)
μ	4.25	4.37	4.02	3.80
θ^b	56	56	52	52
L_b				
E_V (osc.str)	43 300(0.12)	43 600(0.12)	42 400(0.09)	41 900(0.08)
μ	4.87	4.76	5.92	5.81
θ^b	160	158	172	7
$S_{n\pi^*}$				
E_V (osc.str)	45 400(0.00)	45 700(0.00)	45 200(0.00)	44 900(0.00)
μ	3.28	3.30	3.84	3.64
θ^b	102	72	92	89

Notes: [a] State specific calculations. [b] Angle between the transition moment and the molecular axis (see Fig. 1).

As a consequence, since this paper is not aimed to quantitatively reproduce the experimental spectra, we shall base our analysis mainly on 6-31G(d) results, and in order to allow for an easier comparison with the experiments, we shall also report corrected E_V values (E_V^C, λ_A^C on the wavelength scale, the emission energy will be denoted by the subscript E) red-shifted by 2800 cm^{-1}.

In acetonitrile, the relative stability of L_a and L_b states is similar to that predicted in water (see Table 3). In agreement with the experimental spectra, E_V of 9Me-Ade is slightly blue-shifted (~800 cm^{-1}) in acetonitrile with respect to water. Due to the absence of solute–solvent hydrogen bonds, $S_{n\pi^*}$ gets much closer to L_a becoming the second (S_2) adiabatic state. At the 6-31G(d) level it is only 700 cm^{-1} less stable than L_a and a partial mixing between these two states is predicted: indeed $S_{n\pi^*}$ acquires a small but not vanishing oscillator strength and a component in the molecular plane (see Table 3). Increasing the size of the basis set, the energy separation between L_a and $S_{n\pi^*}$ increases (1900 cm^{-1} at the 6-311+G(2d,2p) level) and their coupling decreases.

As shown in Tables S2 and S3 of the ESI,‡ M052X and CAM-B3LYP calculations provide a picture of the FC region similar to that obtained at the PBE0 level.

Excited state deactivation paths. In aqueous solution, starting from the FC region, PBE0 geometry optimizations of L_a predict a very steep path leading to a planar pseudo-minimum

Table 3 Main features of the lowest energy excited states of 9Me-Ade in acetonitrile solution, according to LR-PCM/PBE0 calculations. PCM/PBE0/6-31G (d) geometry optimizations

	6-31G(d)	6-31+G(d,p)	6-31+G(d,p) SS[a]	6-311+G(2d,2p)
L_a				
E_V (osc.str)	41 900(0.22)	41 000(0.30)	41 200(0.21)	40 500(0.29)
μ	3.65	3.52	3.59	3.33
θ^b	54	128	126	52
L_b				
E_V (osc.str)	43 700(0.07)	42 900(0.04)	42 900(0.05)	42 500(0.04)
μ	4.03	4.70	4.36	4.64
θ^b	155	11	21	10
$S_{n\pi^*}$				
E_V (osc.str)	42 600(0.02)	42 600(0.00)	43 400(0.00)	42 400(0.00)
μ	2.1	2.25	2.32	2.18
θ^b	121	70	60	84

Notes: [a] State specific calculations. [b] Angle between the transition moment and the molecular axis (see Fig. 1).

(L_a-min^{*pla}, gradient < 0.0005 a.u.) (see Fig. 6). This minimum is characterized by a significant lengthening of the C2N1 and C2N3 bond lengths, in line with the bonding/antibonding character of the frontier orbitals of 9Me-Ade with respect to those bonds. Emission from L_a-min^{*pla} is fairly intense (oscillator strength = 0.23) at 35 100 cm^{-1} ($\lambda_E \sim 285$ nm, $\lambda_E^C \sim 310$ nm), with a small decrease of the anisotropy ($r = 0.38$, or $r = 0.27$ if also considering L_b contribution to the absorption, see below). It should be noted that our calculations can at the moment only provide qualitative indications of the fluorescence anisotropies, since they depend on several factors: the relative absorption intensities of L_a and L_b at the excitation wavelength, the possibility of partial population transfer and geometry rearrangements on an ultrafast time-scale, *inter alia*, the accurate estimations of which fall outside the scope of the present study. The L_a-min^{*pla} minimum is likely responsible for the experimental emission maximum shown in Fig. 2. However, PBE0 geometry optimizations predict that L_a-min^{*pla} undergoes a rupture of the purine ring planarity, with the C2 atom (see Fig. 1) moving out from the molecular plane, and a partial pyramidalization towards a non-planar structure L_a-min^{C2} (see Fig. 6). The Potential Energy Surface (PES) connecting L_a-min^{*pla} and L_a-min^{C2} is rather flat (the energy difference is only 0.05 eV), but emission from L_a-min^{C2} is significantly red-shifted, with a strong decrease of the oscillator strength ($f = 0.10$): V_E = 28 400 cm^{-1} ($\lambda_E \sim 350$ nm, $\lambda_E^C \sim 390$ nm), and a noticeable decrease of the anisotropy ($r = 0.33$, or $r = 0.22$ if considering also L_b contribution to the absorption). Emission from the region surrounding L_a-min^{C2} could be responsible for the red-tail present, especially in water, in the experimental fluorescence spectrum of dA and 9Me-Ade.

This structure (L_a-min^{C2}) is predicted to be a stationary point on the L_a PES. However, frequency calculations indicate that one very small negative frequency is present, which can be described as a collective librational mode of the 4 water molecules of the first solvation shell associated with an out-of-plane motion of the purine ring.

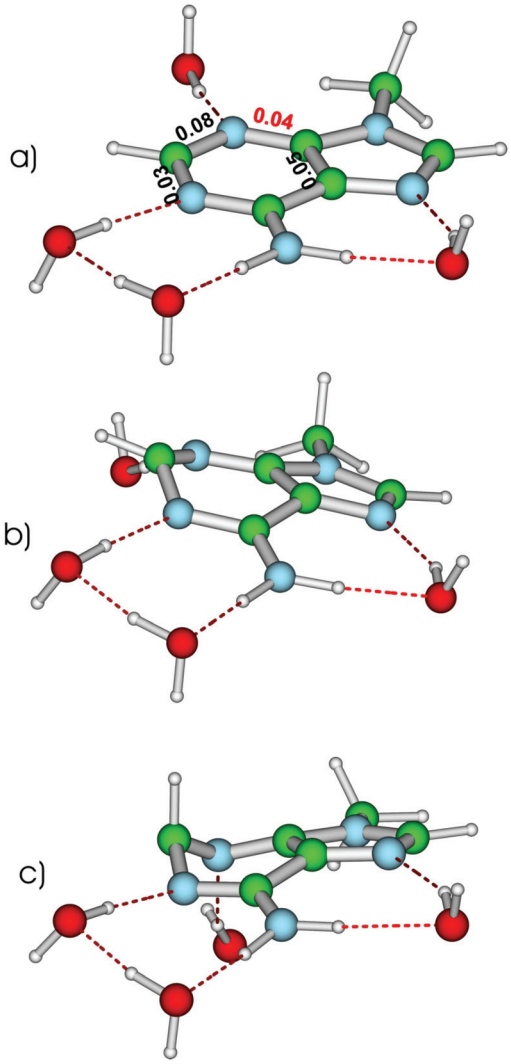

Fig. 6 Schematic drawing of some representative structure of the L_a decay paths in 9Me-Ade·4H_2O. (a) L_a-min^{*pla} pseudo-minimum. The main geometry shifts (in Å) with respect to the S_0 minimum are included (increase in black, decrease in red). (b) L_a-min^{C2} and (c) representative point of the ^{2}E L_a/S_0 crossing region.

We have also investigated the further evolution from L_a-min^{C2}, building the PES associated with the out-of-plane motion of the H2 atom by means of LR-PCM/TD-PBE0/6-31G (d) geometry optimization for different values of the H2–C2–N1–N3 improper dihedral angle (ϕ). After overcoming a small energy barrier (~200 cm^{-1}) for $\phi = 170°$, the energy of L_a decreases steeply and the system decays towards a crossing region with S_0, suggesting the presence of a close-lying conical intersection (CI) (see Fig. 7). The PBE0 picture is therefore fully consistent with the results of post-HF *ab initio* methods in the gas phase, indicating, as anticipated in the introduction, the presence of a L_a/S_0 CI (^{2}E according to the Cremer–Pople notation[90]), involving a large out-of-plane motion of the C2–H2 bond.[27–29]

Geometry optimizations of L_b predict a steep decay to a planar pseudo minimum L_b-min^{*pla} (gradient ~ 0.0005 a.u.),

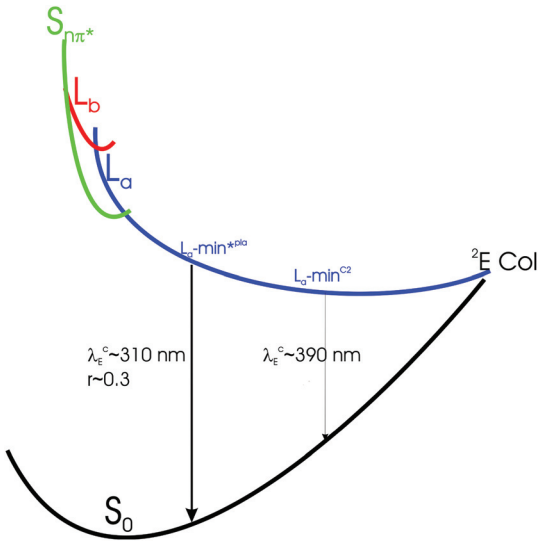

Fig. 7 Schematic description of the main deactivation paths in 9Me-Ade·4H_2O.

and an emission energy of 39 300 cm^{-1} ($\lambda_E \sim 255$ nm, $\lambda_E^C \sim 275$ nm). L_b-min*^{pla} is very close in energy to L_a, which is only 300 cm^{-1} more stable at this point. Indeed, a transition from L_b to L_a is fully plausible, whereafter the system follows the same L_a path as depicted above. This picture is similar to that obtained for guanosine monophosphate,[76] where broad-band transient absorption experiments and QM calculations predict an ultrafast (>100 fs) $L_b \rightarrow L_a$ decay. An ultrafast decay would also decrease the r_0 value, in line with observations.

Geometry optimizations of $S_{n\pi^*}$ predict a very steep decay to a pseudo-minimum ($S_{n\pi^*}$-min*, energy gradient ~0.001 a.u.), which at this point corresponds to the S_1 adiabatic state (La is ~1600 cm^{-1} less stable) characterized by a very large C6C1N2 bond angle (>130°). Emission from $S_{n\pi^*}$-min* is very weak and ν_E = 35 000 cm^{-1} ($\lambda_E \sim 285$ nm, $\lambda_E^C \sim 310$ nm). In analogy with what was found for L_b, a transition from $S_{n\pi^*}$ to L_a is predicted by PCM/TD-PBE0/6-31G(d) geometry optimizations.

TD-M052X calculations predict a qualitatively similar picture. Starting from the FC region a very steep decay on the L_a surface leads to L_a-min*^{pla} followed by a C2 pyramidalization on a much shallower surface. However, at the M052X level, L_a-min^{C2} is not a stationary point, since geometry optimization leads directly to a crossing region with S_0. The key geometry rearrangement involves the H2 atom reaching a close to perpendicular orientation with respect to the molecular plane, indicating a passage to the ^{2}E CI with S_0.

Excited state PBE0 geometry-optimizations of L_a in acetonitrile provide similar results to those obtained in water, with a significant exception. Indeed, at the 6-31G(d) level, geometry optimization indicates the decay of L_a to $S_{n\pi^*}$, and the existence of a real minimum, ($S_{n\pi^*}$-min*) planar, very similar to the pseudo-minimum region just described in water. However, when a larger 6-31+G(d,p) basis set is used, the behaviour of L_a is similar to that obtained in water, with a decay to L_a-min^{C2} (emission at 28 200 cm^{-1}), involving a large out-of-plane motion of the C2–H2 bond, passing through a planar plateau (emission at 35 000 cm^{-1}). The computed fluorescence maxima are therefore similar to those predicted in water. However, with respect to what was found in water the PES leading to La-min^{C2} is steeper and the planar plateau less relevant. A $L_b \rightarrow L_a$ decay is predicted also in acetonitrile.

M052X calculations provide a very similar picture to that just described. At the 6-31G(d) level a $L_a \rightarrow S_{n\pi^*} \rightarrow S_{n\pi^*}$-min* path is found. The only difference with respect to PBE0 results is a slight pyramidalization at C2 predicted for $S_{n\pi^*}$-min*, in analogy with the results of CASSCF geometry optimizations of 6H-adenine in the gas phase. By using a more extended basis set, we find the same picture obtained in water, since geometry optimization leads directly to a L_a/S_0 crossing region *via* a ^{2}E CI.

4. Discussion

As discussed in the introduction, several factors contribute to making a full understanding of the photoexcited dynamics of adenine difficult: the presence of several close lying excited states in the FC region, the accessibility of several potentially operating deactivation paths, the large diabatic couplings existing, especially for non-planar structure, among the different excited states, and solvent effects. This study provides very useful insights into most of the above factors and, therefore, the microscopic processes modulating the excited state decay.

Because most of the oscillator strength is carried by only one transition, L_a, steady state absorption and fluorescence spectra cannot provide stringent evidence for the energy ordering of the lowest energy excited states in the FC region. However, they give one interesting indication, *i.e.* that the spectra exhibit a very small dependence on the solvent, and provide useful data for the validation of our computational approach. In this respect it is comforting that the absorption and emission spectra computed in water and in acetonitrile are in good agreement with experiments.

Our calculations indicate that in water L_a is the lowest energy excited state in the FC region, L_b being ~2000 cm^{-1} less stable. This assignment could be consistent also with the Linear Dichroism measurements in stretched polymer films, which have been interpreted as an indication that L_b is more stable than L_a.[47] Actually, according to Holmén *et al.*[47] the lowest energy transition is polarized roughly along the long molecular axis (as we find for L_a) and S_2 roughly along the short one (as we find for L_b). In any case, in stretched polymer films L_a and $S_{n\pi^*}$ could be significantly mixed in the FC region, making the interpretation of the experimental results less straightforward. Furthermore we do not find any stable minimum on L_b and we predict an ultrafast $L_b \rightarrow L_a$ decay (see Fig. 7). Our calculations thus do not support the interpretation that the fast τ_1 component corresponds to the $L_a \rightarrow L_b$ internal conversion.[59] It is also interesting to note that in this picture there is no ambivalence in applying the Strickler–Berg relation

as previously suggested.[47,59,60,91] The L_a state is dominating both in absorption and in emission.

Our proposal that adenine fluorescence stems essentially from L_a is corroborated by the experimental results. As anticipated above, the computed emission energy agree with the experimental fluorescence maxima and our picture is consistent with the experimental fluorescence anisotropy.

By assuming an ultrafast $L_b \rightarrow L_a$ decay, faster than the present time-resolution ($\approx$ 80 fs), the initial fluorescence anisotropy r_0 would be 0.32 according to LR-PCM/TD-PBE0-6-31G(d) calculations. This is very close to the experimental value, taking into account that the motion of the wavepacket on the L_a surface also induces a decrease of the anisotropy on a very fast time-scale (from 0.40 to 0.36 in the planar plateau and to 0.32 in the L_a-min^{C2}). In this respect, it is noteworthy that the r_0 value for thymidine monophosphate (for which no electronic relaxation occurs) is 0.36.[58] Analogously, red-shifted fluorescence beyond 400 nm mainly stems from the non-planar part of the L_a path, which is characterized by a lower fluorescence anisotropy. This could explain the observed decrease of $r(t)$ at longer wavelengths. On the contrary, as L_a is much more intense than L_b, an $L_a \rightarrow L_b$ decay would cause a much larger decrease of the anisotropy.

The solvent mainly affects the relative energies of L_a and $S_{n\pi^*}$ excited states. In water the possibility of a $L_a \rightarrow S_{n\pi^*}$ population transfer is very small, due to the rather high energy gap, whereas $S_{n\pi^*}$ is predicted to decay to L_a. In contrast to what occurs in the gas phase, our calculations (independently of the adopted functional) indicate that L_a is the only excited state significantly involved in the dynamics. Our prediction is thus in agreement with the results of transient absorption experiments that do not show any significant presence of dark states (identified as $n\pi^*$ states) in adenine.[48] All the experimental fluorescence results can be explained by the shape of the L_a PES, with a steep decay from the FC region towards a planar–plateau, followed by a shallower path towards C2 pyramidalization and the L_a/S_0 ^{2}E CI. The first part of the path is responsible for the fluorescence maximum, while the red-tail is likely due to emission from L_a-min^{C2} or, more generally, the non-planar plateau.

Increasing the excitation wavelength decreases the amount of energy deposited in the excited state and would consequently decrease the 'speed' of the wave-packet in its motion towards the CI, leading to a slightly longer 'residence time' on the non-planar plateau (L_a-min^{C2}). Indeed, Temps and co-workers measured the fluorescence decays of adenosine after excitation between 245 and 274 nm and concluded that the excited state lifetime is independent of the excitation wavelength.[60] However, inspecting their data, there is a small increase from 0.28 to 0.32 ps in the studied wavelength region. In this context, it should be remarked that the dA steady-state fluorescence spectrum does not depend on the excitation wavelength.[58]

The picture emerging from our calculations is similar to that predicted in the gas phase by CASPT2 calculations[27,29] and different from that obtained by Thiel and co-workers by using non-adiabatic semi-classical simulations based on semi-empirical OM2 calculations, predicting a very fast $L_a \rightarrow S_{n\pi^*} \rightarrow S_0$ decay mechanism *via* a $^6S_1$ CI.[53] We cannot exclude that, due the large diabatic coupling, which could be further increased by inclusion of thermal motion and solvent fluctuations, a small part of the photoexcited population is trapped in $S_{n\pi^*}$. Quantum dynamical studies on uracil have shown that population transfer between bright and dark states is possible also when the latter states are less stable than the former by several tenths of eV in the FC region.[92] This part could eventually contribute to the longest living component of the excited state decay, on the ps time scale. On the other hand, our results exclude that the $L_a \rightarrow S_{n\pi^*} \rightarrow S_0$ process plays a significant role in the <1 ps dynamics. The latter mechanism can be consistent with the experimental results only by assuming a barrierless motion through the $^6S_1$ CI. In this context, OM2 calculations have been shown to significantly under-estimate the energy barrier associated with the motion through the $^6S_1$ CI and to produce an extremely short $S_{n\pi^*}$ lifetime (<100 fs).[42] A longer lifetime would make a dark state detectable by transient absorption experiments and would also increase the time during which $S_{n\pi^*}$ is coupled with L_a, with consequences for the steady-state and dynamical fluorescence properties.

The fluorescence decays recorded in acetonitrile are similar to those found in water, and, accordingly, our calculations provide a similar mechanistic picture for the two solvents. The major difference is that a more significant participation of $S_{n\pi^*}$ in the excited state dynamics is possible in acetonitrile, due to the smaller energy gap with L_a. This could explain the 'slowing-down' of the decay in this solvent because a part of the population gets trapped in $S_{n\pi^*}$ before decaying to S_0 'directly' or by back transfer to L_a (as suggested for uracil derivatives).[93] On the other hand, at this stage of our research, it cannot be excluded that the small differences between water and acetonitrile are simply due to some dynamical solvent effect on the $L_a \rightarrow S_0$ decay path.

5. Concluding remarks

In this study we have reported a joint experimental and computational study of the excited state dynamics of dA and 9Me-Ade in water and in acetonitrile. Steady-state and time-resolved fluorescence experiments and quantum mechanical calculations provide a convergent picture of the adenine photophysics in solution. In the Franck–Condon region, the lowest in energy state is the optically bright L_a state, with the L_b state situated about 2000 cm^{-1} higher. Both states are populated when exciting at 267 nm, but the L_b state undergoes an ultrafast $L_b \rightarrow L_a$ decay, too fast for our time-resolution ($\approx$ 80 fs). This is confirmed by the experimentally observed fluorescence anisotropies, attaining low values already at time zero. The excited state relaxation mechanism appears to be ruled by the spectroscopic state L_a in which an almost barrierless path leads from the Franck–Condon region to a conical

intersection with the ground state. We have found that dA and 9Me-Ade exhibit a very similar behaviour, indicating that 9Me-Ade is a valid model for studying dA and AMP excited states.

The excited-state decays in water and acetonitrile are also similar, despite the fact that solute–solvent hydrogen bonds strongly decrease the relative stability of $S_{n\pi^*}$. We have a different picture from that obtained for thymine and 5-fluorouracil (5FU), for which the excited-state decays are significantly faster in acetonitrile than in water.[63,64] For adenine, we find the opposite behaviour, *i.e.* the decays in acetonitrile are somewhat slower than those in water. Interestingly, the same microscopic effect is operative for these compounds: hydrogen bonds destabilize a "dark" $n\pi^*$ state in water, thus rendering a population transfer from the "bright" $\pi\pi^*$ state to $n\pi^*$ state less important. However, for thymine and 5-fluorouracil the direct decay of the "bright" $\pi\pi^*$ state to S_0 is significantly slower than that of the L_a state of adenine. Furthermore, in pyrimidines the coupling between the "dark" and "bright" states is likely less effective, *i.e.* the population transferred to the "dark" state is clearly non-radiative. Time-resolved fluorescence experiments of pyrimidines indicated a faster decay of the "bright" $\pi\pi^*$ state in acetonitrile, where the $\pi\pi^* \rightarrow n\pi^*$ channel is operative, than in water. Indeed, transient absorption experiments (which can monitor the presence of "dark" states) on pyrimidines in acetonitrile show the presence of a long-lived "dark" state (identified as an $n\pi^*$ state) and a slowing-down of the global excited state decay (in analogy with what we found for adenine). These considerations confirm that it is not easy to derive general rules for predicting solvent effects on different spectral observables. The excited state decay depends on the interplay between different kinds of effects, both intrinsic and environmental. Depending on the relative stability of two excited states, a hydrogen bonding solvent can either increase or decrease their energy difference with regard to the gas phase. Furthermore, different experimental techniques are sensitive to diverse molecular properties, and thus they can monitor the different excited states with varying sensibility. More important, even for a single excited state, different regions of the PES can produce very different signals depending on the spectroscopic technique.

Acknowledgements

R.I. thanks MIUR (FIRB 2008 Futuro in Ricerca and PRIN 2010–2011) for financial support. The French Agency for Research (ANR-10-BLAN-0809-01, "DNAExciton") is acknowledged for financial support. Financial support from the Spanish Government (JCI-2011-09926 and Salvador Madariaga Program (grant to M.C.J.)) is gratefully acknowledged.

References

1 C. E. Crespo-Hernández, B. Cohen, P. M. Hare and B. Kohler, *Chem. Rev.*, 2004, **104**, 1977–2020.
2 C. E. Crespo-Hernández, B. Cohen and B. Kohler, *Nature*, 2005, **436**, 1141–1144.
3 C. T. Middleton, K. de La Harpe, C. Su, Y. K. Law, C. E. Crespo-Hernandez and B. Kohler, *Annu. Rev. Phys. Chem.*, 2009, **60**, 217–239.
4 T. Gustavsson, R. Improta and D. Markovitsi, *J. Phys. Chem. Lett.*, 2010, **1**, 2025–2030.
5 D. Markovitsi, T. Gustavsson and I. Vaya, *J. Phys. Chem. Lett.*, 2010, **1**, 3271–3276.
6 M. K. Shukla and J. Leszczynski, *J. Biomol. Struct. Dyn.*, 2007, **25**, 93–118.
7 N. K. Schwalb and F. Temps, *Science*, 2008, **322**, 243–245.
8 L. Serrano-Andrés and M. Merchán, *J. Photochem. Photobiol., C*, 2009, **10**, 21–32.
9 D. Markovitsi, T. Gustavsson and A. Banyasz, *Mutat. Res.-Rev. Mutat. Res.*, 2010, **704**, 21–28.
10 T. Gustavsson, A. Banyasz, R. Improta and D. Markovitsi, *J. Phys.: Conf. Ser.*, 2011, 261.
11 B. Bouvier, T. Gustavsson, D. Markovitsi and P. Millié, *Chem. Phys.*, 2002, **275**, 75–92.
12 E. R. Bittner, *J. Photochem. Photobiol., A-Chem.*, 2007, **190**, 328–334.
13 I. Buchvarov, Q. Wang, M. Raytchev, A. Trifonov and T. Fiebig, *Proc. Natl. Acad. Sci. U. S. A.*, 2007, **104**, 4794–4797.
14 E. B. Starikov, G. Cuniberti and S. Tanaka, *J. Phys. Chem. B*, 2009, **113**, 10428–10435.
15 A. W. Lange and J. M. Herbert, *J. Am. Chem. Soc.*, 2009, **131**, 3913–3922.
16 F. Santoro, V. Barone and R. Improta, *J. Am. Chem. Soc.*, 2009, **131**, 15232–15245.
17 Y. Lu, Z. G. Lan and W. Thiel, *Angew. Chem., Int. Ed.*, 2011, **50**, 6864–6867.
18 L. B. Clark, G. G. Peschel and I. Tinoco, *J. Phys. Chem.*, 1965, **69**, 3615–3618.
19 N. J. Kim, G. Jeong, Y. S. Kim, J. Sung, S. K. Kim and Y. D. Park, *J. Chem. Phys.*, 2000, **113**, 10051–10055.
20 D. C. Lührs, J. Viallon and I. Fischer, *Phys. Chem. Chem. Phys.*, 2001, **3**, 1827–1831.
21 E. Nir, K. Kleinermanns, L. Grace and M. S. d. Vries, *J. Phys. Chem. A*, 2001, **105**, 5106–5110.
22 C. Plützer, E. Nir, M. S. d. Vries and K. Kleinermanns, *Phys. Chem. Chem. Phys.*, 2001, **3**, 5466.
23 E. Nir, C. Plützer, K. Kleinermanns and M. d. Vries, *Eur. Phys. J. D: Atom., Mol. and Opt. Phys.*, 2002, **20**, 317–329.
24 C. Plützer and K. Kleinermanns, *Phys. Chem. Chem. Phys.*, 2002, **4**, 4877–4882.
25 N. J. Kim, H. Kang, Y. D. Park and S. K. Kim, *Phys. Chem. Chem. Phys.*, 2004, **6**, 2802–2805.
26 S. Perun, A. L. Sobolewski and W. Domcke, *J. Am. Chem. Soc.*, 2005, **127**, 6257–6265.
27 L. Serrano-Andres, M. Merchán and A. C. Borin, *Proc. Natl. Acad. Sci. U. S. A.*, 2006, **103**, 8691–8696.
28 L. Serrano-Andres, M. Merchán and A. C. Borin, *Chem.–Eur. J.*, 2006, **12**, 6559–6571.

29 I. Conti, M. Garavelli and G. Orlandi, *J. Am. Chem. Soc.*, 2009, **131**, 16108–16118.
30 S. Ullrich, T. Schultz, M. Z. Zgierski and A. Stolow, *J. Am. Chem. Soc.*, 2004, **126**, 2262–2263.
31 S. Ullrich, T. Schultz, M. Z. Zgierski and A. Stolow, *Phys. Chem. Chem. Phys.*, 2004, **6**, 2796–2801.
32 C. Canuel, M. Mons, F. Piuzzi, B. Tardivel, I. Dimicoli and M. Elhanine, *J. Chem. Phys.*, 2005, **122**, 0743161–0743166.
33 C. Canuel, M. Elhanine, M. Mons, F. Piuzzi, B. Tardivel and I. Dimicoli, *Phys. Chem. Chem. Phys.*, 2006, **8**, 3978–3987.
34 H.-H. Ritze, H. Lippert, E. Samoylova, V. R. Smith, I. V. Hertel, W. Radloff and T. Schultz, *J. Chem. Phys.*, 2005, **122**, 224320.
35 C. Z. Bisgaard, H. Satzger, S. Ullrich and A. Stolow, *ChemPhysChem*, 2009, **10**, 101–110.
36 M. Barbatti and H. Lischka, *J. Am. Chem. Soc.*, 2008, **130**, 6831–6839.
37 E. Fabiano and W. Thiel, *J. Phys. Chem. A*, 2008, **112**, 6859–6863.
38 Y. B. Lei, S. A. Yuan, Y. S. Dou, Y. B. Wang and Z. Y. Wen, *J. Phys. Chem. A*, 2008, **112**, 8497–8504.
39 R. Mitric, U. Werner, M. Wohlgemuth, G. Seifert and V. Bonacic-Koutecky, *J. Phys. Chem. A*, 2009, **113**, 12700–12705.
40 M. Barbatti, A. J. A. Aquino, J. J. Szymczak, D. Nachtigallová, P. Hobza and H. Lischka, *Proc. Natl. Acad. Sci. U. S. A.*, 2010, **107**, 21453–21458.
41 A. N. Alexandrova, J. C. Tully and G. Granucci, *J. Phys. Chem. B*, 2010, **114**, 12116–12128.
42 M. Barbatti, Z. Lan, R. Crespo-Otero, J. J. Szymczak, H. Lischka and W. Thiel, *J. Chem. Phys.*, 2012, **137**, 22A503.
43 D. Voet, W. B. Gratzer, R. A. Cox and P. Doty, *Biopolymers*, 1963, **1**, 193–208.
44 R. F. Stewart and N. Davidson, *J. Chem. Phys.*, 1963, **39**, 255–266.
45 P. R. Callis, *Annu. Rev. Phys. Chem.*, 1983, **34**, 329–357.
46 W. Voelter, R. Records, E. Bunnenbe and C. Djerassi, *J. Am. Chem. Soc.*, 1968, **90**, 6163–6170.
47 A. Holmén, A. Broo, B. Albinsson and B. Nordén, *J. Am. Chem. Soc.*, 1997, **119**, 12240–12250.
48 P. M. Hare, C. E. Crespo-Hernández and B. Kohler, *Proc. Natl. Acad. Sci. U. S. A.*, 2007, **104**, 435–440.
49 S. Yamazaki and S. Kato, *J. Am. Chem. Soc.*, 2007, **129**, 2901–2909.
50 V. Ludwig, Z. M. da Costa, M. S. do Amaral, A. C. Borin, S. Canuto and L. Serrano-Andrés, *Chem. Phys. Lett.*, 2010, **492**, 164–169.
51 B. Mennucci, A. Toniolo and J. Tomasi, *J. Phys. Chem. A*, 2001, **105**, 4749–4757.
52 R. Improta and V. Barone, *Theor. Chem. Acc.*, 2008, **120**, 491–497.
53 Z. G. Lan, Y. Lu, E. Fabiano and W. Thiel, *ChemPhysChem*, 2011, **12**, 1989–1998.
54 I. Conti, P. Altoe, M. Stenta, M. Garavelli and G. Orlandi, *Phys. Chem. Chem. Phys.*, 2010, **12**, 5016–5023.
55 J.-M. L. Pecourt, J. Peon and B. Kohler, *J. Am. Chem. Soc.*, 2000, **122**, 9348–9349.
56 J. Peon and A. H. Zewail, *Chem. Phys. Lett.*, 2001, **348**, 255–262.
57 T. Gustavsson, A. Sharonov, D. Onidas and D. Markovitsi, *Chem. Phys. Lett.*, 2002, **356**, 49–54.
58 D. Onidas, D. Markovitsi, S. Marguet, A. Sharonov and T. Gustavsson, *J. Phys. Chem. B*, 2002, **106**, 11367–11374.
59 W.-M. Kwok, C. Ma and D. L. Phillips, *J. Am. Chem. Soc.*, 2006, **128**, 11894–11905.
60 T. Pancur, N. K. Schwalb, F. Renth and F. Temps, *Chem. Phys.*, 2005, **313**, 199–212.
61 B. Cohen, P. M. Hare and B. Kohler, *J. Am. Chem. Soc.*, 2003, **125**, 13594–13601.
62 T. Gustavsson, A. Banyasz, E. Lazzarotto, D. Markovitsi, G. Scalmani, M. J. Frisch, V. Barone and R. Improta, *J. Am. Chem. Soc.*, 2006, **128**, 607–619.
63 T. Gustavsson, N. Sarkar, E. Lazzarotto, D. Markovitsi, V. Barone and R. Improta, *J. Phys. Chem. B*, 2006, **110**, 12843–12847.
64 T. Gustavsson, N. Sarkar, E. Lazzarotto, D. Markovitsi and R. Improta, *Chem. Phys. Lett.*, 2006, **429**, 551–557.
65 F. Santoro, V. Barone, T. Gustavsson and R. Improta, *J. Am. Chem. Soc.*, 2006, **128**, 16312–16322.
66 F. Santoro, T. Gustavsson, A. Lami, V. Barone and R. Improta, Towards the understanding of the excited state dynamics of nucleic acids: solvent and stacking effects on the photophysical behavior of nucleobases, *AIP Conference Proceedings*, 2007, vol. 963, pp. 631–634.
67 T. Gustavsson, A. Banyasz, N. Sarkar, D. Markovitsi and R. Improta, *Chem. Phys.*, 2008, **350**, 186–192.
68 T. Gustavsson, A. Sharonov and D. Markovitsi, *Chem. Phys. Lett.*, 2002, **351**, 195–200.
69 C. Adamo and V. Barone, *J. Chem. Phys.*, 1999, **110**, 6158–6170.
70 Y. Zhao, N. E. Schultz and D. G. Truhlar, *J. Chem. Theor. Comput.*, 2006, **2**, 364–382.
71 T. Yanai, *Chem. Phys. Lett.*, 2004, **393**, 51–57.
72 R. Improta, in *Computational Strategies for Spectroscopy: from Small Molecules to Nanosystems*, ed. V. Barone, John Wiley & Sons, Chichester, 2011, pp. 39–76.
73 D. Jacquemin, E. A. Perpete, I. Ciofini and C. Adamo, *Acc. Chem. Res.*, 2009, **42**, 326–334.
74 A. Banyasz, S. Karpati, Y. Mercier, M. Reguero, T. Gustavsson, D. Markovitsi and R. Improta, *J. Phys. Chem. B*, 2010, **114**, 12708–12719.
75 F. Santoro, V. Barone and R. Improta, *Proc. Natl. Acad. Sci. U. S. A.*, 2007, **104**, 9931–9936.
76 V. Karunakaran, K. Kleinermanns, R. Improta and S. A. Kovalenko, *J. Am. Chem. Soc.*, 2009, **131**, 5839–5850.
77 R. Improta, *Phys. Chem. Chem. Phys.*, 2008, **10**, 2656–2664.
78 F. Santoro, V. Barone and R. Improta, *ChemPhysChem*, 2008, **9**, 2531–2537.
79 R. Improta and V. Barone, *Angew. Chem., Int. Ed.*, 2011, 12016–12019.
80 A. Banyasz, T. Gustavsson, D. Onidas, P. Changenet-Barret, D. Markovitsi and R. Improta, *Chem.–Eur. J.*, 2013, **19**, 3762–3774.

81 M. Dargiewicz, M. Biczysko, R. Improta and V. Barone, *Phys. Chem. Chem. Phys.*, 2012, **14**, 8981–8989.
82 L. Biemann, S. A. Kovalenko, K. Kleinermanns, R. Mahrwald, M. Markert and R. Improta, *J. Am. Chem. Soc.*, 2011, **133**, 19664–19667.
83 J. Tomasi, B. Mennucci and R. Cammi, *Chem. Rev.*, 2005, **105**, 2999.
84 G. Scalmani, M. J. Frisch, B. Mennucci, J. Tomasi, R. Cammi and V. Barone, *J. Chem. Phys.*, 2006, **124**, 094107.
85 R. Improta, V. Barone, G. Scalmani and M. J. Frisch, *J. Chem. Phys.*, 2006, **125**, 054103.
86 R. Improta, G. Scalmani, M. J. Frisch and V. Barone, *J. Chem. Phys.*, 2007, **127**, 074504.
87 M. J. Frisch, G. W. Trucks, H. B. Schlegel, G. E. Scuseria, M. A. Robb, J. R. Cheeseman, J. J. A. Montgomery, T. Vreven, K. N. Kudin, J. C. Burant, J. M. Millam, S. S. Iyengar, J. Tomasi, V. Barone, B. Mennucci, M. Cossi, G. Scalmani, N. Rega, G. A. Petersson, H. Nakatsuji, M. Hada, M. Ehara, K. Toyota, R. Fukuda, J. Hasegawa, M. Ishida, T. Nakajima, Y. Honda, O. Kitao, H. Nakai, M. Klene, X. Li, J. E. Knox, H. P. Hratchian, J. B. Cross, V. Bakken, C. Adamo, J. Jaramillo, R. Gomperts, R. E. Stratmann, O. Yazyev, A. J. Austin, R. Cammi, C. Pomelli, J. W. Ochterski, P. Y. Ayala, K. Morokuma, G. A. Voth, P. Salvador, J. J. Dannenberg, V. G. Zakrzewski, S. Dapprich, A. D. Daniels, M. C. Strain, O. Farkas, D. K. Malick, A. D. Rabuck, K. Raghavachari, J. B. Foresman, J. V. Ortiz, Q. Cui, A. G. Baboul, S. Clifford, J. Cioslowski, B. B. Stefanov, G. Liu, A. Liashenko, P. Piskorz, I. Komaromi, R. L. Martin, D. J. Fox, T. Keith, M. A. Al-Laham, C. Y. Peng, A. Nanayakkara, M. Challacombe, P. M. W. Gill, B. Johnson, W. Chen, M. W. Wong, C. Gonzalez and J. A. Pople, *GAUSSIAN 09 (Revision A.02)*, Gaussian, Inc., Wallingford CT, 2009.
88 F. A. Miannay, T. Gustavsson, A. Banyasz and D. Markovitsi, *J. Phys. Chem. A*, 2010, **114**, 3256–3263.
89 F. J. Avila Ferrer, J. Cerezo, E. Stendardo, R. Improta and F. Santoro, *J. Chem. Theor. Comput.*, 2013, **9**, 2072–2082.
90 D. Cremer and J. A. Pople, *J. Am. Chem. Soc.*, 1975, **97**, 1354–1358.
91 B. Cohen, C. E. Crespo-Hernández and B. Kohler, *Faraday Discuss. Chem. Soc.*, 2004, **127**, 137–147.
92 R. Improta, V. Barone, A. Lami and F. Santoro, *J. Phys. Chem. B*, 2009, **113**, 14491–14503.
93 Y. Mercier, F. Santoro, M. Reguero and R. Improta, *J. Phys. Chem. B*, 2008, **112**, 10769–10772.

